Size-selected Pt Nanoparticles Synthesized via Micelle Encapsulation: Effect of Pretreatment and Oxidation State on the Activity for Methanol Decomposition and Oxidation

Jason R. Croy[a], S. Mostafa[a,b], H. Heinrich[a,c], B. Roldan Cuenya[a,b,d*]

[a]Department of Physics, [b]Department of Civil and Environmental Engineering, [c]Center of Advanced Materials Processing and Characterization, [d]Nanoscience Technology Center, University of Central Florida, Orlando, Fl 32816

* Corresponding Author

Email: roldan@physics.ucf.edu

Abstract

The effect of pretreatment conditions on the oxidation state and activity of micelle-synthesized Pt nanoparticles supported on ZrO_2 was studied for methanol decomposition and oxidation reactions. An O_2-pretreatment is observed to be effective for producing clean, stable, and active nanoparticles. Pt-oxide species formed during such pretreatments were found to have little influence in methanol decomposition reactions due to their tendency to reduce. However, these same species are stable during methanol oxidation and appear to take part in a Mars-van Krevelen-type of process, in which bound-oxygen (nanoparticle shell) may be replenished with oxygen from the gas phase.

Keywords: Pt nanoparticles, micelles, methanol decomposition, methanol oxidation, Pt oxide, PtO, PtO_2, ZrO_2, XPS, TEM, AFM, mass spectrometry, packed-bed reactor.

Introduction

In the last two decades it has become evident that highly dispersed metal nanoparticles (NPs) supported on oxides display unique catalytic properties. Novel geometric as well as electronic effects present in small particles (<10 nm) give rise to the intriguing physical and chemical properties of these systems [1-5]. Furthermore, interaction of the NPs with the support oxide may be significant and likewise contribute to the observed catalytic performance [6-16]. However, one of the major challenges in working with such catalysts is the difficulty in producing highly dispersed NPs with controllable size and spatial distributions. This becomes important in light of the fact that NP size can influence activity [17-20] and selectivity [3] as well as the stability of some metal-oxide species [4, 17, 21, 22], which might themselves present enhanced chemical reactivities [23]. In addition, the favorable reduction of surface energy by an increase in NP size (i.e. thermal sintering) must be minimized during catalysts preparation and subsequent exposure to chemical reactants [24]. This minimization may be facilitated by proper choice of support [7, 25, 26], and/or interparticle distances when using planar substrates [27]. An additional concern is the cleanliness of the catalytically active component (e.g. precious metal) which is dictated by the preparation method and may vary from one technique to the next [28, 29]. Although many advances have been made and a number of NP synthesis routes are available [26, 28-32], not many adequately meet the criteria with respect to the goal of reliably controlling all parameters (i.e. size, spatial distribution, stability, oxidation state). Furthermore, proprietary methods are often not fully disclosed leading to conflicting results for seemingly similar systems [31]. One technique receiving increasing interest is that of micelle encapsulation. This technique is

based on the self-assembly of diblock copolymers into micelles which serve as sites for NP formation via the introduction of a metal precursor (i.e. H_2PtCl_6) [7, 17, 33, 34]. The advantages of this technique lie in the ability to produce small NPs with narrow size and spatial distributions [27, 35-37] as well as easily accommodating various metals and bimetallic compositions [34, 36, 38]. On polycrystalline powder supports, the disadvantage lies in the difficulty of completely removing the encapsulating polymer, along with precursor elements such as Cl, without broadening too much the initially narrow size distribution. Chlorine is known to be a poison for Pt in oxidation reactions [31] and its removal is dependent on temperature and choice of support [17, 39]. With planar substrates thermal effects (i.e. sintering) may be overcome by use of low-temperature polymer removal treatments such as gas plasmas (O_2 and H_2) [22, 35]. However, micelle-encapsulated NPs deposited on nanocrystalline oxide powders by way of impregnation techniques require high temperature calcination procedures (>450°C) to ensure clean NP catalysts [17]. Therefore, NP-support combinations which not only facilitate reactions but also promote stability against agglomeration are necessary. To further complicate the situation, drying times and temperatures as well as the ambient conditions of calcination (temperature, time, gases present, flow of gases, etc.) have an influence on the final oxidation state of the catalyst.

Recently, much attention has been directed towards the oxidation state of active metal catalysts and whether or not oxidized metals may be beneficial with respect to their reduced counterparts. As such, the interaction of various chemicals with oxidized surfaces have been investigated and some interesting results obtained [22, 40-43]. For example, the adsorption of MeOH on Cu is found to be greatly enhanced by oxygen [44],

either in the feed gas or as part of the catalyst due to an incomplete reduction process [45]. Over et al. [23] showed that the $RuO_2(110)$ surface is highly active for CO oxidation and oxidized Ru is also preferred over its metallic state in bimetallic Pt-Ru anode catalysts for fuel cell applications [46]. PtO_2 surfaces have also been reported to be more active for CO oxidation than metallic Pt [47] and theoretical work by Gong et al.[48] shows that $RuO_2(110)$, $RhO_2(110)$, $PdO_2(110)$, $OsO_2(110)$, $IrO_2(110)$ and $PtO_2(110)$ are indeed more reactive than the corresponding metal surfaces for CO oxidation. Recent work by Friend's group on O-covered Au(111) also demonstrates the enhanced reactivity of the pre-oxidized gold surface [49, 50]. It thus appears that the traditional negative view of oxidation as a process leading to reduced catalytic performance must be reconsidered [51]. However, in the case of Pt there seems to be a debate regarding the benefits of Pt oxides. For example, the temporal decay in the performance of Pt-based fuel cell electrodes has been attributed to the formation of PtO and Pt dissolution [52]. On the other hand, there also exist a number of reports suggesting that the presence of Pt-oxides could have a positive effect on catalytic performance. Dam al. [53] have shown that Pt dissolution reaches a saturation level due to the presence of a protective platinum oxide layer. Further, a study by Hull et al. [54] shows enhanced activity for Pt-carbon nanotubes catalysts, where the Pt particles are covered by a thin Pt oxide shell. Although for any particular application there will be reaction-specific considerations, the ability to synthesize systems with predetermined, stable final oxidation states is clearly desirable.

In this study we address the open question of whether or not Pt-oxides may play some significant role with respect to catalytic activity in their interaction with MeOH. Micelle-synthesized, monometallic Pt NPs supported on ZrO_2 powder were used as

catalysts. Specific emphasis has been placed on the pretreatment conditions in order to obtain samples of high purity with narrow size distributions and distinct contents of Pt oxide species. The effect of the pretreatment conditions on the oxidation state and activity of our micellar Pt NPs has been tested for MeOH decomposition and oxidation reactions. Our data demonstrate that the oxides of Pt show drastic differences in their stability for the different reactions. The first part of our discussion will focus on sample preparation/characterization and subsequently on the performance of these samples for MeOH decomposition and oxidation. We are particularly interested in addressing the following specific questions: i) what are the best pre-treatment conditions for optimizing the catalytic performance of micelle-synthesized NPs, ii) to what degree, and under which conditions, are the different oxides of Pt in our systems stable, and (iii) how does the presence of Pt-oxide species affect the reactivity of our Pt/ZrO_2 nanocatalysts.

2. Experimental

2.1 Catalyst synthesis and pretreatment

Non-polar/polar diblock copolymers [Poly(styrene)-block-poly(2vinylpyridine) Polymer Source Inc.] were dissolved in a non-polar solvent (toluene) in order to obtain a solution of spherical nano-cages known as inverse micelles. The solution was then loaded with Pt in the form of a metal salt ($H_2PtCl_6 \cdot 6H_2O$) to produce self-confined and size-selected Pt NPs. The particle size was controlled by using a polymer with a specific head length [PS(27700)-PVP(4300), i.e. constant PVP molecular weight for all samples] and by selecting a metal-salt/polymer-head (PVP) molar ratio of 0.3 [4, 20, 33]. The solution was then mixed with nanocrystalline ZrO_2 (~ 45 nm grain size, Alfa Aesar) in the form of

a powder resulting in a loading of 1% wt Pt. The sample was stir-dried in air at ~ 100°C for 48 hours, after which four different calcination experiments under different gaseous atmospheres were carried out, each utilizing a fresh 110 mg sample of the dried Pt-salt/ZrO_2 powder. The four pretreatments were each carried out at 500°C on four analogously prepared fresh samples and included calcination in: i) a flow of O_2 for 8 hours, ii) a flow of helium for 8 hours, iii) a flow of H_2 for 8 hours, and iv) a flow of O_2 for 4 hours followed by a flow of H_2 for 2 hours. All flows were 50 ml/min total with the O_2 and H_2 treatments containing 50% O_2 or H_2 respectively and balanced with helium. All gas-flow treatments were done in a packed-bed reactor as described below.

2.2 Morphological and structural characterization

Transmission electron microscopy (TEM) measurements were carried out on the powder samples with a Tecnai F30 TEM operating at an accelerating voltage of 300 kV. In parallel to TEM studies, the polymer-salt solutions were also dip-coated on SiO_2/Si(001) substrates in order to obtain particle size information (height) via atomic force microscopy (AFM) with a Nanoscope Multimode (Digital Instruments) microscope operating in tapping mode.

2.3 Electronic and chemical characterization

The powder samples were transferred to an ultra high vacuum system (UHV, SPECS GmbH) for analysis by X-ray photoelectron spectroscopy (XPS) immediately after the different ex-situ pretreatments as well as after exposure to MeOH. The sample transfer time between our mass flow reactor and the ultra high vacuum XPS system was

less than 15 min. XPS data were collected using a monochromatic X-ray source (Al-Kα, 1486.6 eV) operating at 350 W, and a flood gun was used to correct for sample charging during measurements. All spectra were referenced to the Zr $3d_{5/2}$ [ZrO_2] peak at 182.6 eV [55]. The fits of the Pt-4f spectra were done after Shirley background subtraction using asymmetric Gausian-Lorentzian line-shapes (Casa XPS software). An asymmetry index of 0.2 was obtained for the Pt^0 $4f_{7/2}$ in all fits, in agreement with the 0.19 value reported in the literature for bulk Pt-4f [56]. For each spectrum the ratio of the two XPS lines in the Pt-4f spin-orbit coupling doublet (Pt-$4f_{7/2}$ and $4f_{5/2}$) and their difference in energy were held constant at the theoretical values of 0.75 and 3.3 eV respectively. The spectra were fitted with three doublets corresponding to metallic Pt ($4f_{7/2}$ ~71.7 eV), PtO ($4f_{7/2}$ ~73.1 eV) and PtO_2 ($4f_{7/2}$ ~75.3 eV) [57]. The maximum width (FWHM) of each component was held constant [Pt^0 (1.6 eV), PtO (1.8 eV), PtO_2 (1.9 eV)] from spectrum to spectrum. A tolerance of ± 0.2 eV was allowed in order to account for broadening associated with changing concentrations, for example, after significant reduction of $Pt^{\delta+}$ species. For comparison, the FWHM of our Zr $3d_{5/2}$ reference peak is ~ 1.4 eV. This makes the FWHM assignments given above for Pt species reasonable as Pt makes up only 1% of the total sample weight compared to the ZrO_2 support material.

2.4 Reactivity characterization

Catalytic decomposition/oxidation of methanol in the vapor phase was carried out in a packed-bed mass flow reactor with a vertical stainless steel tube (inner diameter = 7.4 mm) serving as the reactor vessel. A thermocouple (K-type) in contact with the outside wall of the reactor, at the position of the catalyst, was used to monitor

temperature and the entire assembly was insulated to minimize heat losses. Immediately following the above pretreatments the reactor was flushed with helium and activities for MeOH decomposition and oxidation reactions were measured at atmospheric pressure at a temperature of 260°C (decomposition) and at 260°C and 50°C (oxidation), each for a period of 4 hours. Mass flow controllers (MKS) were used to flow helium through a stainless steel bubbler (containing MeOH) as well as a bubbler-bypass line which was used to control the concentration of MeOH. The total flow was 50 ml/min resulting in a MeOH flow of 38 μmol/min for decomposition and oxidation reactions. MeOH oxidation was carried out in an excess of O_2 with an O_2/MeOH ratio of ~ 2. Reactions were monitored by a quadrupole mass spectrometer (QMS, Hiden HPR20), details of which can be found in Ref. [17]. The entrance of the mass spectrometer is attached to a heated capillary tube which inhibits condensation, and all lines are heated at ~ 150°C during experiments. Sixteen different masses were monitored to identify and distinguish reactant and product gases. In order to ensure the reproducibility of the acquired data, each experiment was conducted twice with fresh samples and the average values reported. The experimental error bars displayed correspond to the difference of the reactivity values obtained from the two measurements. For reference purposes, the reactivity of the stainless steel reactor (loaded with the inert quartz wool) was tested within the temperature range of our experiments (≤ 260°C). Under these conditions, a maximum of approximately 3 % MeOH conversion was obtained at 260°C and 50°C for MeOH decomposition and oxidation reactions, respectively.

3. Results and Discussion:

3.1 Morphological and structural characterization (AFM, TEM)

The morphology of our micellar Pt nanoparticles was studied by AFM. Figure 1(a) displays an AFM image of the nanoparticle polymeric solution dip-coated on SiO_2/Si(001). Figure 1(b) shows particles after the removal of the encapsulating polymer by and in-situ (UHV) O_2-plasma treatment. It is clear from these images that our synthesis technique allows for a high level of control and results in Pt NPs having a narrow size distribution. Analysis of image 1(b) gives an average particle size (AFM height) of 2.1 ± 0.4 nm.

Figure 2 displays high resolution TEM images of our NP samples after annealing for 8 hours in O_2 (a-c), He (d-f), and H_2 (g-i). The images in Fig. 2(a-f) reveal the presence of crystalline NPs. The average NP diameters obtained by TEM are: 4.2 ± 0.7 (8 hours O_2), 4.4 ± 0.7 nm (8 hours He), and 3.3 ± 0.8 nm (8 hours H_2). These average particles sizes (TEM diameters) are about twice the value of those measured by AFM (height) after polymer removal by an in-situ O_2-plasma treatment, Fig. 1(b). Likewise, from Fig. 2 we see that our particles are somewhat oblate rather than spherical. This is evidence that the micelle encapsulated particles form a strong contact with the ZrO_2 support [see region marked by an arrow in Fig. 2(e)] and do not significantly coalesce when treated under H_2, He, and O_2, even at high temperatures (500°C). The analysis of high-resolution TEM images of NPs in Fig. 2 gives a lattice parameter of ~3.91 ± 0.04 Å for NPs annealed in O_2 [Fig. 3(b)], and an average value of 3.94 ± 0.04 Å after annealing in He [Figs. 3(d), (e) and (f), respectively]. This average value was obtained from two sets of {111} planes and one set of {200} planes. All of our samples appear to be

polymer-free with the exception of the sample annealed in H_2, Fig. 2(g-i), where a thin amorphous shell enveloping the NPs as well as the ZrO_2 support is observed [highlighted by arrows in Figs. 2(g,i)]. This observation is attributed to the presence of a residual polymeric shell (C-coating) on this sample. Due to this surface coating, no lattice parameter could be extracted from these images. As will be discussed later, this TEM observation is in agreement with a significant residual C signal in the XPS spectrum of this sample.

3.2 Electronic and compositional characterization (XPS)

A) Effect of sample pre-treatment

Figure 3 shows XPS spectra from the Pt-4f core level region of the Pt NPs deposited on nanocrystalline ZrO_2 powder directly after the different pretreatments but before exposure to methanol. The vertical lines in Fig. 3 mark the positions of the $4f_{7/2}$ peak of metallic Pt (solid line), Pt^{2+} in PtO (dashed line), and Pt^{4+} in PtO_2 (dashed line) at the energies given in the experimental section. The relative content of the different Pt species obtained from the analysis of the data in Fig. 3 are summarized in Table 1. The estimated error for the calculated areas of the fitted components given in Table 1 is ± 3 %. The distinction between PtO and PtO_2 species based on XPS binding energies (BEs) can be difficult, especially when considering the wide range of energies that have been reported [57]. NPs can further complicate things due to low peak intensities and the associated peak broadening. However, a monochromatic X-ray source was used for these measurements to minimize peak broadening, and the BEs and energy separations obtained from our spectral fits are in agreement with previously published data [57-60].

Nevertheless, the metallic Pt-$4f_{7/2}$ peak in our Pt NPs is shifted ~ 0.7 eV higher than the value of bulk Pt [61]. This positive shift may be attributed to final state effects in our small clusters and/or an interaction with the support itself [62]. One possible interaction is the formation of interfacial Pt-Zr compounds. Jung et al. [63] have studied the interfacial properties of ZrO_2-supported precious metals using DFT calculations for Pt_4, Pd_4, and Rh_4 clusters on the surface of ZrO_2(111). They found the adsorption of Pt to be associated with the largest surface rearrangement and strong Pt-Zr interaction as well as Pt-O bond formation. The same authors also report that oxidation of their clusters increased the metal-support interaction [63]. In addition, their calculations revealed a charge transfer from metal atoms in the clusters to the support and a polarization of the deposited clusters, consistent with our observed positive BE shifts. We also see from the TEM images evidence of this strong particle-support interaction. For example, the He treated sample of Fig. 2(e) shows the substrate drawn up and around the perimeter of the nanoparticle-support interface (region highlighted by an arrow). In addition, even though our initial encapsulating micelles were spherical, most particles imaged show some degree of flattening at the support interface after annealing at 500°C as in Fig. 2(e), highlighting strong particle-support interactions. However, since the lattice parameter of a Pt_3Zr alloy (3.99 Å [64]) is close to that of Pt (3.96 Å), distinguishing pure Pt from Pt-Zr compounds is a difficult task, specially considering our experimental TEM error ~0.04 Å . In addition, much of the alloying is expected to take place at the particle-support interface, and the TEM values that we have obtained (3.91-3.94 Å) were averaged over entire particles.

From Table 1 and Fig. 3 we see that the sample treated in a flow of O_2 for 8 hours consists of ~25 % Pt^0, ~57 % PtO, and ~18 % PtO_2 indicating that the dominant component is PtO. We have shown in a previous study [34] that PtO in Pt/ZrO_2 NP systems is the preferentially formed oxide, especially in Pt particles greater than ~ 2 nm, in agreement with Wang et al. [65]. Furthermore, PtO appears to be stable in this system, and as will be shown below, cannot be completely reduced even under our reaction conditions for MeOH decomposition, Fig. 4.

The possibility of detecting Pt^{2+} and Pt^{4+} species by way of chlorides (residues from the H_2PtCl_4 salt in the NP preparation) instead of Pt oxide formation has been considered. If stable, such species would show XPS peaks at ~ 73.6 eV and ~ 75.5 eV for the $4f_{7/2}$ of $PtCl_2$ and $PtCl_4$ respectively [57], which are similar values to the PtO and PtO_2 BEs. Unfortunately, the main XPS peak for Cl (2p) resides at ~ 200 eV, a BE where the ZrO_2 support also shows a feature, rendering the identification of residual Cl in the Pt/ZrO_2 samples difficult. However, the absence of Cl in our samples after all the different annealing treatments at 500°C can be concluded based on: (i) the lack of a Cl signal in analogous micellar Pt nanoparticles deposited on TiO_2, Al_2O_3, CeO_2, and SiO_2 (where the support does not show an XPS peak in the Cl-2p region) after annealing at 500°C [7, 17], and (ii) the fact that the high BE Pt-4f peaks are present on the samples annealed under an oxidizing environment (O_2).

The samples annealed in flows of H_2 and helium are considerably reduced and consist of mainly metallic Pt, with both samples reducing to ~ 90 % Pt^0. Furthermore, there seems to be a limit of reducibility for our samples (~ 90 % Pt^0), since complete reduction was not observed even after MeOH exposure in decomposition reactions at

260°C, Fig. 4 and Table 1. The 10 % content of Pt oxides present in these samples is assigned to stable Pt-O-Zr species at the Pt/ZrO_2 interface. Interestingly, once our samples had been reduced (H_2 treatment), a subsequent air exposure for 48 hours resulted in minimal reoxidation (from ~94 % to 84 % Pt^0). This experiment also corroborates that our ex-situ XPS data are not significantly affected by the short transfer time (~ 15 min) which takes place after calcination and/or reaction between the pre-treatment chamber (mass flow reactor) and the surface analysis UHV system.

B) Stability of Pt oxides

We have investigated by XPS the stability of Pt oxides in our Pt/ZrO_2 nanocatalysts after direct MeOH decomposition (Fig. 4) and MeOH oxidation (Fig. 5) reactions. We can see from the analysis given in Table 1 that the Pt^{4+} (PtO_2) component has been completely reduced in all samples after direct methanol decomposition, Fig. 4. However, as seen in Fig. 3 and Table 1, even reduction in a flow of H_2 does not completely eliminate PtO from these catalysts (~9 %). A possible explanation for the stability of this oxidized Pt species is the strong interaction between Pt atoms at the interface of the NPs and the ZrO_2 substrate as discussed above. Nagai et al. [66] have recently shown the importance of the Pt-O-support bond strength in the re-dispersion of agglomerated Pt-based automotive catalysts. Here, the mobility of Pt and Pt oxide species, dictated by the choice of support, leads to the possibility of catalyst regeneration and increased lifetime. PtOx species that form on large, sintered particles become mobile and can re-disperse over the surface where they are stabilized because of the strong interaction between Pt and the support [66]. Another possibility for the incomplete reduction of oxides in our NPs is the

presence of subsurface as well as surface oxide species. Surface oxide species may be more easily decomposed upon gas exposure whereas subsurface components can remain stable, especially when deposited on non-reducible oxides [22]. Yazakawa et al. [67] have also noted that Pt supported on ZrO_2 is difficult to reduce when compared to other supports which are more acidic (i.e. SiO_2-Al_2O_3). The authors also reported that the stability of these oxides is responsible for the inferior performance of their Pt/ZrO_2 catalyst in the combustion of methane as compared to more easily reducible systems. In addition, it should be noted that even though our oxidized Pt species were formed upon annealing in an oxygen-rich environment at 500°C, our experimental reaction temperature of 260°C during MeOH exposure is relatively low, and significant thermal decomposition of our oxides is not expected under these circumstances. For example, temperature programmed desorption studies of pre-oxidized Pt(111) surfaces utilizing an atomic oxygen beam revealed O_2 desorption features at temperatures as high as 500°C [68].

From Table 1 we see that after MeOH decomposition reactions most samples reduce to fairly similar final states, with ~5-13 % PtO detected after MeOH exposure at 260°C. Our MeOH decomposition experiments result in the catalysts being exposed to MeOH at 260°C for four hours followed immediately by XPS measurements. In order to further investigate the stability of Pt oxide species in our samples during direct methanol decomposition, a test was conducted in which a sample was exposed to MeOH at 260°C for only a short time interval (10 min) followed immediately by XPS measurements. For this test a new sample was prepared by pre-treating it with O_2 for four hours at 500°C (for polymer removal and oxidation), and then exposing it to MeOH from room temperature

up to the reaction temperature of 260°C with a heating ramp of 8°C/min (XPS spectrum not shown). Our XPS data showed that this sample was also reduced to a maximum value of ~90 % Pt^0. This is evidence that the oxides in our samples are not chemically stable under MeOH exposure and reduce rather quickly, most likely due to the presence of CO upon MeOH decomposition. This idea is supported by the detection of CO_2 in all MeOH decomposition experiments as will be noted in the reactivity section. Similar observations were also made for thin films of oxidized Rh exposed to MeOH at 200-350°C [69].

The stability of Pt oxide species during MeOH oxidation reactions was also evaluated. Different sample pretreatments were carried out on a second batch of samples, before MeOH oxidation, in order to obtain samples with different contents of Pt^0 and Pt-oxides (Table 1). The treatments included: i) O_2 annealing for 4 hours at 500°C (polymer removal) plus H_2 reduction at 500°C for 2 hours, ii) O_2 annealing for 4 hours at 500°C plus reduction via the decomposition of MeOH at 260°C for 4 hours (as shown in Fig. 4 and Table 1), and iii) O_2 annealing for 8 hours at 500°C. Figure 5 shows XPS of the Pt-4f core level region for these Pt/ZrO_2 samples before (bottom spectrum, 4 hours O_2 treatment only) and after MeOH oxidation reactions at 50°C and 260°C. Table 1 gives the corresponding results of the XPS analysis. The spectrum of the as-prepared sample (annealed for 4 hours in O_2) indicates that this sample is highly oxidized and Table 1 shows that it contains oxide concentrations analogous to the sample treated for 8 hrs in oxygen shown in Fig. 3. This suggests that a limit to the oxidation of these particles under our conditions has been reached after four hours. Contrary to the results displayed in Fig. 4, where all samples appeared mainly reduced after MeOH decomposition reactions, Fig. 5 indicates that exposure of oxidized NPs to MeOH + O_2 at 50°C does not result in the

reduction of $Pt^{\delta+}$ species. Nevertheless, when the MeOH oxidation temperature was increased to 260°C, a small decomposition (~14 %) of the PtO component was observed. From these data we see that both samples remain in highly oxidized states after reaction. These results are opposite for the case of MeOH decomposition reactions in which the oxides were found to be chemically unstable. In the presence of oxygen the oxides of Pt remain relatively stable at least up to 260°C during MeOH oxidation. Wang et al. [70] have also reported a slight stabilization of AgO_x species under MeOH oxidation conditions.

The two samples that were reduced in H_2 and subjected to MeOH oxidation at 50°C and 260°C did not display changes with respect to their oxidation state after reaction, Table 1. The same applies to the sample reduced during MeOH decomposition and subsequently exposed to MeOH and O_2 at 50°C, Table 1. All three samples contain mainly metallic Pt, although none of our samples were found to completely reduce under any of our reaction conditions. We note here the possibility that highly active sites on the surface of our NPs may be prone to rapid re-oxidation upon air exposure, therefore, even though transfer times are less than 15 min, this process cannot be ruled out as responsible for the small Pt oxide contents detected on the H_2 and MeOH reduced samples.

3.3 Reactivity (Mass spectrometry)

A) MeOH decomposition: activity and selectivity

Figure 6 shows the rate of MeOH conversion at 260°C for differently treated Pt/ZrO_2 samples given in μmol(MeOH)converted/s/g·Pt. Conversions listed are at the beginning of each reaction run, however, no significant deactivation was found for these

samples. The main products observed for all Pt/ZrO_2 samples were CO and H_2 indicating the direct decomposition of MeOH given by:

$$CH_3OH \Leftrightarrow CO + 2H_2 \qquad (1)$$

The Pt-free ZrO_2 substrate (not shown), after a 4 hour pretreatment in O_2, was found to give ~5 % conversion at 260°C with small amounts of CO, H_2, CO_2, methyl formate ($HCOOCH_3$), and water as products. For comparison with Fig. 6, the rate of the ZrO_2 support normalized to grams of ZrO_2 is ~ 0.3 μmol(MeOH)converted/s/g ·ZrO_2 All Pt/ZrO_2 samples showed small amounts of CO_2, which might be attributed to reactions occurring at the ZrO_2 support, to the water-gas-shift (WGS) reaction, and/or to the reduction of Pt-oxides by CO in the case of pre-oxidized samples. The low levels of CO_2 detected make a deconvolution of these processes difficult.

The addition of Pt to the ZrO_2 support almost eliminated completely the production of methyl formate at 260°C in all samples. Instead, methyl formate was detected at low temperatures, (~100°C) prior to reaching the target temperature of 260°C, at which point only trace levels of this gas could be observed.

It can be seen from Fig. 6 that the H_2 treatment leads to a sample having the lowest activity for MeOH decomposition. This is attributed to the insufficient removal of the encapsulating polymer, as evidenced in the TEM images of Figs. 2(g-i), resulting in a contaminated catalyst surface before MeOH exposure. Figure 7 shows XPS spectra of the C-1s core level region of our NPs before (solid curves) and after (open symbols) MeOH decomposition reactions. The arrows labeled C_p span a range of energies representative of carbon associated with the polymer used in the synthesis of the NPs [71]. The dashed lines represent CO bound to Pt in bridged and linear configurations at 285.6 eV and 286.3

eV respectively [72]. Before reaction (solid curves) all samples except the H_2-treated sample show negligible amounts of carbon, with a very broad peak (low intensity) around ~285.2 eV. This energy is typical of adventitious carbon. The $O_2 + H_2$ sample shows the lowest C signal before the reaction with MeOH, while a clear C peak was observed on the H_2-treated sample before reaction, Fig. 8 (top solid curve). Considering the range of binding energies taken up by polymeric carbon (C_p), we assign the large C signal of the latter sample to an insufficient removal of the polymeric shell from our NPs. This indicates clearly that annealing in H_2 is not an efficient way of cleaning micelle-synthesized NPs, and that the amorphous layer covering this sample observed in the TEM images of Fig. 2(g-i) is certainly of carbonaceous origin. In this case, hydrogen can react with O and N in PVP suppressing the reactions between N and O with C, and leading to an incomplete removal of polymer-related carbonaceous species.

Figure 6 and Table 1 might suggest that an increased presence of Pt-oxides in the O_2 exposed samples could be responsible for improved reactivity. However, an additional test was conducted on our samples consisting of a H_2 pretreatment (2 hours at 500°C) after the initial O_2 exposure (4 hours at 500°C). Even though the H_2 treated sample contained a lower amount of Pt oxides (32 % PtO and 5% PtO_2, Table 1), it turned out to be the most active from the entire series. This result could be due to several reasons: (i) the exposure to H_2 induces changes in the structure and reactivity of the NPs, or (ii) once the encapsulating polymer has been completely removed by the O_2 treatment, the subsequent H_2 exposure serves to reduce the NPs and metallic Pt species are more reactive than oxidized species for the direct decomposition of methanol. The C-1s XPS data in Fig. 7 indicate a very small background C signal in this sample, and the spectra

acquired before and after MeOH exposure are nearly identical. However, similar results were also obtained on the sample annealed in O_2 for 8 hours, indicating that the presence of a lower content of residual polymeric carbon in this sample cannot explain its improved reactivity. With respect to the effect of H_2, it has been reported for Pd [73] that the presence of surface H_2 enhances the decomposition of methoxy groups, which is regarded as the rate limiting step for MeOH decomposition in several systems including Pd, Cu, and Pt [73-77]. This could explain the superior activity of the $O_2 + H_2$ treated sample. This enhanced activity might also be due to the improved reactivity of metallic Pt, as compared to Pt-oxides, simply due to the H_2 reduction process. However, our MeOH-decomposition-ramp experiment (annealing from room temperature to 260°C with a heating rate of 8°C/min) revealed that these samples are already reduced beyond the point of the H_2 treated sample by the time we reach the reaction temperature of 260°C. This suggests that it is not just metallic Pt that plays a role in the observed activity of this sample but that H_2, on or incorporated into the surface, might also have a positive influence in the decomposition of MeOH. In order to corroborate this point, we tried reducing our samples by a treatment in O_2 + He at 500°C, but found that they contain ~25 % less metallic Pt than the $O_2 + H_2$ samples, making a direct comparison of similar systems impossible.

From the above results we can conclude that the oxides of Pt play no significant role in the decomposition of MeOH over these catalysts, as they are chemically unstable in the presence of MeOH at 260°C.

B) MeOH oxidation: activity and selectivity

The MeOH oxidation reactions were carried out in an excess of oxygen with an O_2/MeOH ratio of ~ 2 (see eq. 2) while maintaining a total flow of 50 ml/min (38 µmol/min MeOH) as in the decomposition reactions. For all oxidation reactions CO_2 and water are the main products detected suggesting the complete oxidation of MeOH via reaction (2).

$$CH_3OH + \frac{3}{2}O_2 \Leftrightarrow CO_2 + 2H_2O \qquad (2)$$

The ZrO_2 support (pretreated in O_2 for 4 hours at 500°C) shows a conversion of ~ 27 % with the additional products of methyl formate and dimethyl ether appearing in small amounts. This is in agreement with observations of Hu et al. [78] for ZrO_2 supports in their study of supported molybdenum oxide catalysts and is also an indication of zirconia's acid-base properties [79]. All Pt/ZrO_2 samples showed 100 % conversion of MeOH when the oxidation reaction was carried out at 260°C accompanied by the disappearance of methyl formate and dimethyl ether.

Fig. 8 shows the rate of MeOH conversion in µmol(MeOH)converted/s/g·Pt at 50°C for the different sample pretreatments. We can see that there is virtually no difference in activity, under our reaction conditions, for the oxidized versus the reduced samples, each showing ~ 93-96 % MeOH conversion at 50°C. For comparison, the Pt-free ZrO_2 substrate had a rate of ~2.0 µmol(MeOH)converted/s/g· ZrO_2 at this temperature.

It is interesting that the initial state of the catalyst is maintained for all samples after oxidation reactions, Fig. 5 and Table 1. For example, the reduced samples remained reduced while the oxidized samples remained oxidized. For oxidation at 50°C the

concentration of Pt species is virtually unaffected, however, for oxidation reactions at 260°C we see an overall reduction of the oxides of ~9% and even a small increase (~5%) in the PtO_2 component suggesting additional oxidation beyond the initial treatment. It has been noted that pure Pb surfaces are quite resistant to oxidation, however, oxide formation can be stimulated by impurities, and once nucleated PbO can actually catalyze the growth of additional oxides in an autocatalytic process [80]. It has also been shown that a RuO_2 film grows autocatalytically on the Ru(0001) surface [81]. A similar situation may exist in our Pt/ZrO_2 catalysts in which a highly reduced Pt surface will not easily re-oxidize, but when Pt-oxide species dominate the particle composition they may take part in a Mars-van Krevelen-type of process whereby oxygen depleted from the catalyst surface is replenished by gas-phase O_2. Support for this mechanism is also evident in the ~90 % reduction of all samples after decomposition reactions with MeOH, i.e. in the absence of gas-phase O_2 all samples reduce (Table 1), however, even after oxidation reactions at 260°C the oxides of Pt remain.

Conclusions

The present study highlights the importance that the sample pretreatment has on the removal of residual contaminants from the sample preparation method, the oxidation state, and subsequent reactivity of colloidal (polymeric) Pt nanoparticles. We have demonstrated that micelle-encapsulated Pt NPs supported on ZrO_2 can be calcined at 500°C under a flow of oxygen for relatively long times without noticeable coarsening, and that such a pre-treatment is highly efficient for the removal of polymeric carbon leading to highly reactive and thermally stable nanocatalysts. Pretreatments in the

presence of different gases lead to differing degrees of oxidation with micelle encapsulated NPs forming strong contacts with the ZrO_2 support. This latter idea is reinforced by the observed, highly stable Pt-O compounds, most likely at the NP-support interface, which do not fully reduce under our reaction conditions or H_2 treatments. In addition, we observe that O_2-treated samples exposed to H_2 before reaction are the most active for the decomposition of MeOH, likely due to promotional effects of H_2 in the decomposition of methoxy species.

The complete oxidation of MeOH takes place over our catalyst in the presence of excess oxygen at 50°C with no appreciable difference in activity for oxidized versus reduced samples and 100 % conversion for all samples is obtained at 260°C regardless of pre-treatment. This is evidence that the oxidized surfaces of our Pt NPs are active for the oxidation of MeOH and reduction pre-treatments commonly reported in the literature may not be necessary. Furthermore, the oxidized surface appears to take part in a Mars-van Krevelen-type of process, exchanging oxygen from the particle's Pt oxide shell with gas-phase O_2, allowing it to remain oxidized during/after MeOH oxidation reactions.

Acknowledgments

The authors would like to thank Robert Croy for his technical assistance. This work was made possible thanks to the financial support of the US Department of Energy, Office of Basic Energy Sciences, DE-FG02-08ER15995.

References

[1] C.T. Campbell, Science 306 (2004) 234.

[2] M. Mavrikakis, P. Stoltze and J. Norskov, Catal. Lett. 64 (2000) 101.

[3] M. Haruta, Catal. Today 36 (1997) 153.

[4] B. Roldan Cuenya, S.H. Baeck, T.F. Jaramillo and E.W. McFarland, J. Am. Chem. Soc. 125 (2003) 12929.

[5] T.V. Choudhary and D.W. Goodman, Top. Catal. 21 (2002) 25.

[6] A.M. Argo, J.F. Odzak, F.S. Lai and B.C. Gates, Nature 415 (2002) 623.

[7] J.R. Croy, S. Mostafa, J. Liu, Y.H. Sohn, H. Heinrich and B. Roldan Cuenya, Catal. Lett. 119 (2007) 209.

[8] M. Haruta, CATTECH 6 (2002) 102.

[9] Y. Men, H. Gnaser, R. Zapf, V. Hessel and C. Ziegler, Catal. Commun. 5 (2004) 671.

[10] A. Badri, C. Binet and J.C. Lavalley, J. Chem. Soc. Faraday Trans. 92 (1996) 1603.

[11] B.R. Powell and S.E. Whittington, J. Catal. 81 (1983) 382.

[12] O. Dulub, W. Hebenstreit and U. Diebold, Phys. Rev. Lett. 84 (2000) 3646.

[13] A.V. Ivanov and L.M. Kustov, Russ. Chem. B 47 (1998) 1061.

[14] L.M. Molina and B. Hammer, Appl. Catal. A 291 (2005) 21.

[15] J.A. Rodriguez, G. Liu, T. Jirsak, J. Hrbek, Z.P. Chang, J. Dvorak and A. Maiti, J. Am. Chem. Soc. 124 (2002) 5242.

[16] M. Kurtz, J. Strunk, O. Hinrichsen, M. Muhler, K. Fink, B. Meyer and C. Wöll, Angew. Chem. Int. Edit. 44 (2005) 2790.

[17] J.R. Croy, S. Mostafa, J. Liu, Y.H. Sohn and B. Roldan Cuenya, Catal. Lett. 118 (2007) 1.

[18] M. Valden, X. Lai and D.W. Goodman, Science 281 (1998) 1647.

[19] M. Haruta and Y. Souma, Catal. Today 36 (1997) 1.

[20] L.K. Ono, D. Sudfeld and B. Roldan Cuenya, Surf. Sci. 600 (2006) 5041.

[21] H.G. Boyen, G. Kästle, F. Weigl, B. Koslowski, C. Dietrich, P. Ziemann, J.P. Spatz, S. Riethmuller, C. Hartmann, M. Möller, G. Schmid, M.G. Garnier and P. Oelhafen, Science 297 (2002) 1533.

[22] L.K. Ono and B. Roldan Cuenya, J. Phys. Chem. C 112 (2008) 4676.

[23] H. Over, Y.D. Kim, A.P. Seitsonen, S. Wendt, E. Lundgren, M. Schmid, P. Varga, A. Morgante and G. Ertl, Science 287 (2000) 1474.

[24] S.C. Parker and C.T. Campbell, Phys. Rev. B 75 (2007) 035430.

[25] G.R. Bamwenda, S. Tsubota, T. Nakamura and M. Haruta, Catal. Lett. 44 (1997) 83.

[26] M.S. Spencer and M.V. Twigg, Annu. Rev. Mater. Res. 35 (2005) 427.

[27] L.K. Ono and B. Roldan-Cuenya, Catal Lett 113 (2007) 86.

[28] J. Libuda, S. Schauermann, M. Laurin, T. Schalow and H.J. Freund, Monatshefte für Chemie 136 (2005) 59.

[29] J.A. Schwarz, C. Contescu and A. Contescu, Chem. Rev. 95 (1995) 477.

[30] U. Heiz and U. Landman, *Nanocatalysis*, (Springer, Heidelberg, 2007).

[31] J. Regalbuto, *Catalyst Preparation*, (CRC Press, Boca Raton, 2007).

[32] N. Zheng, J. Fan and G.D. Stucky, J. Am. Chem. Soc. 128 (2006) 6550.

[33] J.P. Spatz, S. Mossmer, C. Hartmann, M. Möller, T. Herzog, M. Krieger, H.G. Boyen, P. Ziemann and B. Kabius, Langmuir 16 (2000) 407.

[34] J.R. Croy, S. Mostafa, L. Hickman, H. Heinrich and B. Roldan Cuenya, Appl. Cat. A 350 (2008) 207.

[35] G. Kästle, H.G. Boyen, F. Weigl, G. Lengl, T. Herzog, P. Ziemann, S. Riethmuller, O. Mayer, C. Hartmann, J.P. Spatz, M. Möller, M. Ozawa, F. Banhart, M.G. Garnier, and P. Oelhafen, Adv. Func. Mater. 13 (2003) 853.

[36] A. Naitabdi and B. Roldan Cuenya, App. Phys. Lett. 91 (2007) 113110.

[37] J.P. Spatz, A. Roescher and M. Möller, Adv. Mater. 8 (1996) 337.

[38] A. Naitabdi, L.K. Ono, F. Behafarid and B.Roldan Cuenya, J. Phys. Chem. C 113 (2009) 1433.

[39] S.D. Jackson, J. Willis, G.D. Mclellan, G. Webb, M.B.T. Keegan, R.B. Moyes, S. Simpson, P.B. Wells and R. Whyman, J. Catal. 139 (1993) 191.

[40] Y. Xu, J. Greeley and M. Mavrikakis, J. Am. Chem. Soc. 127 (2005) 12823.

[41] X. Wang, W.-K. Chen and C.-H. Lu, Appl. Surf. Sci. 254 (2008) 4421.

[42] I.E. Wachs and R.J. Madix, J. Catal. 53 (1978) 208.

[43] D.R. Rolison, P.L. Hagans, K.E. Swider and J.W. Long, Langmuir 15 (1999) 774.

[44] A.F. Carley, A.W. Owens, M.K. Rajumon, M.W. Roberts and S.D. Jackson, Catal. Lett. 37 (1996) 79.

[45] S.T. Yong, K. Hidajat and S. Kawi, Catal. Today 131 (2008) 188.

[46] K. Lasch, L. Jorissen, K.A. Friedrich and J. Garche, J. Solid State Electrochem. 7 (2003) 619.

[47] B.L.M. Hendriksen and J.W.M. Frenken, Phys. Rev. Lett. 89 (2002) 046101.

[48] X.Q. Gong, Z.P. Liu, R. Raval and P. Hu, J. Am. Chem. Soc. 126 (2004) 8.

[49] X.Y. Deng, B.K. Min, X.Y. Liu and C.M. Friend, J. Phys. Chem. B 110 (2006) 15982.

[50] B.K. Min, A.R. Alemozafar, D. Pinnaduwage, X. Deng and C.M. Friend, J. Phys. Chem. B 110 (2006) 19833.

[51] H. Over and A.P. Seitsonen, Science 297 (2002) 2003.

[52] H.A. Gasteiger, S.S. Kocha, B. Sompalli and F.T. Wagner, Appl. Catal. B 56 (2005) 9.

[53] V.A.T. Dam and F.A. de Bruijn, J. Electrochem. Soc. 154 (2007) B494.

[54] R.V. Hull, L. Li, Y.C. Xing and C.C. Chusuei, Chem. Mater. 18 (2006) 1780.

[55] B.V. Crist, *On-Screen PDF Handbook of Monochromatic XPS Spectra - Commercially Pure Binary Oxides*, XPS International Inc., 2005, Vol.2, p. 828.

[56] S. Tougaard and A. Ignatiev, Surf. Sci. 124 (1983) 451.

[57] NIST X-ray Photoelectron Spectroscopy Database, Version 3.4 (Web Version) http://srdata.nist.gov/xps/index.htm

[58] J. Croy, S. Mostafa, L. Hickmann, H. Heinrich and B. Roldan Cuenya, Appl. Cat. A 350 (2008) 207.

[59] A.S. Arico, A.K. Shukla, H. Kim, S. Park, M. Min and V. Antonucci, Appl. Surf. Sci. 172 (2001) 33.

[60] A.K. Shukla, M. Neergat, P. Bera, V. Jayaram and M.S. Hegde, J. Electroanal. Chem. 504 (2001) 111.

[61] J.L.G. Fierro, J.M. Palacios, F. Tomas, Surf. Interface Anal. 13 (1988) 25.

[62] A. Howard, D.N.S. Clark, C.E.J. Mitchell, R.G. Egdell and V.R. Dhanak, Surf. Sci. 518 (2002) 210.

[63] C.H. Jung, R. Ishimoto, H. Tsuboi, M. Koyama, A. Endou, M. Kubo, C.A. Del Carpio and A. Miyamoto, Appl. Catal. A 305 (2006) 102.

[64] K. Schubert, S. Bhan, T.K. Biswas, K. Frank and P.K. Panday, Naturwiss. 55 (1968) 542.

[65] C.B. Wang and C.T. Yeh, J. Catal. 178 (1998) 450.

[66] Y. Nagai, K. Dohmae, Y. Ikeda, N. Takagi, T. Tanabe, N. Hara, G. Guilera, S. Pascarelli, M.A. Newton, O. Kuno, H.Y. Jiang, H. Shinjo, S. Matsumoto, Angew. Chem. Int. Ed. 47 (2008) 9303.

[67] Y. Yazawa, N. Kagi, S. Komai, A. Satsuma, Y. Murakami and T. Hattori, Catal. Lett. 72 (2001) 157.

[68] J.F. Weaver, J.J. Chen and A.L. Gerard, Surf. Sci. 592 (2005) 83.

[69] C.T. Williams, C.G. Takoudis and M.J. Weaver, J. Phys. Chem. B 102 (1998) 406.

[70] C.B. Wang, G. Deo and I.E. Wachs, J. Phys. Chem. B 103 (1999) 5645.

[71] G. Beamson and D. Briggs, *High Resolution XPS of Organic Polymers - The Scienta ESCA300 Database*, (John Wiley & Sons, New York, 1992).

[72] O. Pozdnyakova, D. Teschner, A. Wootsch, J. Krohnert, B. Steinhauer, H. Sauer, L. Toth, F.C. Jentoft, A. Knop-Gericke, Z. Paal, and R. Schlögl, J. Catal. 237 (2006) 1.

[73] S. Shiizaki, I. Nagashima, Y. Matsumura and M. Haruta, Catal. Lett. 56 (1998) 227.

[74] Y.H. Zhou, P.H. Lv and G.C. Wang, J. Mol. Catal. A 258 (2006) 203.

[75] Y. Matsumura, M. Okumura, Y. Usami, K. Kagawa, H. Yamashita, M. Anpo and M. Haruta, Catal. Lett. 44 (1997) 189.

[76] S. Imamura, T. Hagashihara, Y. Saito, H. Aritani, H. Kanai, Y. Matsumura and N. Tsuda, Catal. Today 50 (1999) 369.

[77] J. Greeley and M. Mavrikakis, J. Catal. 208 (2002) 291.

[78] H.C. Hu and I.E. Wachs, J. Phys. Chem. 99 (1995) 10911.

[79] J.M. Tatibouet, Appl. Catal. A 148 (1997) 213.

[80] K. Thurmer, E. Williams and J. Reutt-Robey, Science 297 (2002) 2033.

[81] H. Over, A.P. Seitsonen, E. Lundgren, M. Schmid and P. Varga, Surf. Sci. 515 (2002) 143.

Table 1 – Relative phase content of the different Pt and Pt-oxide species from the Pt-4f XPS spectra shown in Figs. 3, 4 and 5. This table contains data obtained after different sample pre-treatments and after MeOH decomposition and oxidation reactions.

Pre-treatment		**Pt^0 (%)**	**PtO(%)**	**PtO_2 (%)**
8 hours O_2	Before MeOH	25.2	57.2	17.6
	After MeOH decomposition	86.8	13.2	0
4 hours O_2	Before MeOH	24.3	55.6	20.1
	After MeOH oxidation, 50°C	25.0	56.3	18.7
	After MeOH oxidation, 260°C	32.9	41.9	25.2
4 hours O_2 + 2 hours H_2	Before MeOH	63.8	31.7	4.5
	After MeOH decomposition	88.7	11.3	0
	After MeOH oxidation, 50°C	65.6	29.0	5.4
	After MeOH oxidation, 260°C	62.3	31.7	6.0
Reduction in MeOH	After MeOH oxidation, 50°C	90.0	10.0	0
8 hours He	Before MeOH	86.6	13.4	0
	After MeOH decomposition	93.9	6.1	0
8 hours H_2	Before MeOH	90.9	9.1	0
	After MeOH decomposition	94.3	5.7	0
	Before MeOH, after 48 hours air	83.6	12.6	3.8

Figure Captions

Figure 1 –AFM images of Pt NPs synthesized by micelle encapsulation and deposited on SiO_2/Si(001) taken (a) before and (b) after polymer removal via an in-situ (UHV) O_2-plasma treatment.

Figure 2 – TEM images of Pt NPs deposited on nanocrystalline ZrO_2 powder. (a)-(c) show particles from the sample annealed in a flow of O_2 for 8 hours, (d-f) in a flow of He for 8 hours, and (g-i) in a flow of H_2 for 8 hours.

Figure 3 – XPS spectra of the Pt-4f region of Pt NPs deposited on ZrO_2 powder following the different pretreatments as listed on the right hand side of the graph. The vertical reference lines indicate the binding energies of the $4f_{7/2}$ peaks of Pt^0 (solid line), PtO (dashed line), and PtO_2 (dashed line). Each pretreatment was conducted on a separate, fresh sample.

Figure 4 – XPS spectra of the Pt-4f region of Pt NPs deposited on ZrO_2 powder following the different pretreatments indicated on the right-hand side and subsequent reaction with MeOH at 260°C for 4 hours. The vertical reference lines indicate the binding energies of the $4f_{7/2}$ peaks of Pt^0 (solid line), PtO (dashed line), and PtO_2 (dashed line). Each pretreatment and reaction was conducted on a separate, fresh sample.

Figure 5 – XPS spectra of the Pt-4f region of Pt NPs deposited on ZrO_2 powder following the different pretreatments listed on the left hand side of the graph and subsequent MeOH oxidation. The vertical reference lines represent the $4f_{7/2}$ peaks of Pt^0 (solid line), PtO (dashed line), and PtO_2 (dashed line). Each pretreatment and reaction was conducted on a separate, fresh sample.

Figure 6 – Rate of MeOH decomposition at 260°C for all Pt/ZrO2 samples given in µmol(MeOH)/s/g·Pt. Pretreatments applied to each sample are listed on the graph. Each pretreatment and reaction was conducted on a separate, fresh sample.

Figure 7 – XPS spectra of the C-1s region of all samples before (solid lines) and after (open symbols) reaction with MeOH. C_p is a range of binding energies where C associated with polymers used in the NP synthesis may be found. The dashed lines represent CO bound to Pt in bridged and linear configurations at 285.6 eV and 286.3 eV respectively. The pretreatments applied to each sample are listed along the left hand side of the graph. Each pretreatment was conducted on a separate, fresh sample before interaction with MeOH.

Figure 8 – Rate of MeOH conversion given in µmol(MeOH)converted/s/g·Pt during oxidation reactions at 50°C for the Pt/ZrO_2 NPs pretreated in oxygen, and reduced in hydrogen and MeOH. Each pretreatment and reaction was conducted on a separate, fresh sample.

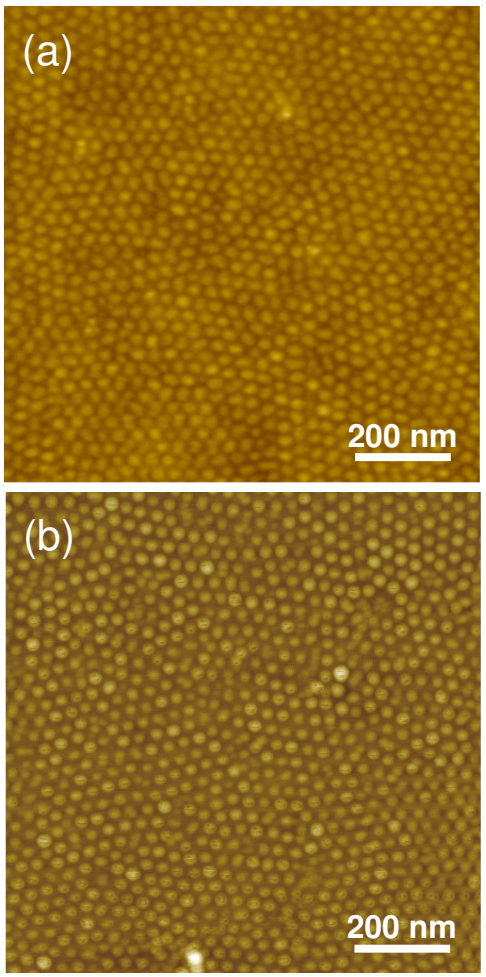

Croy et al., Fig. 1

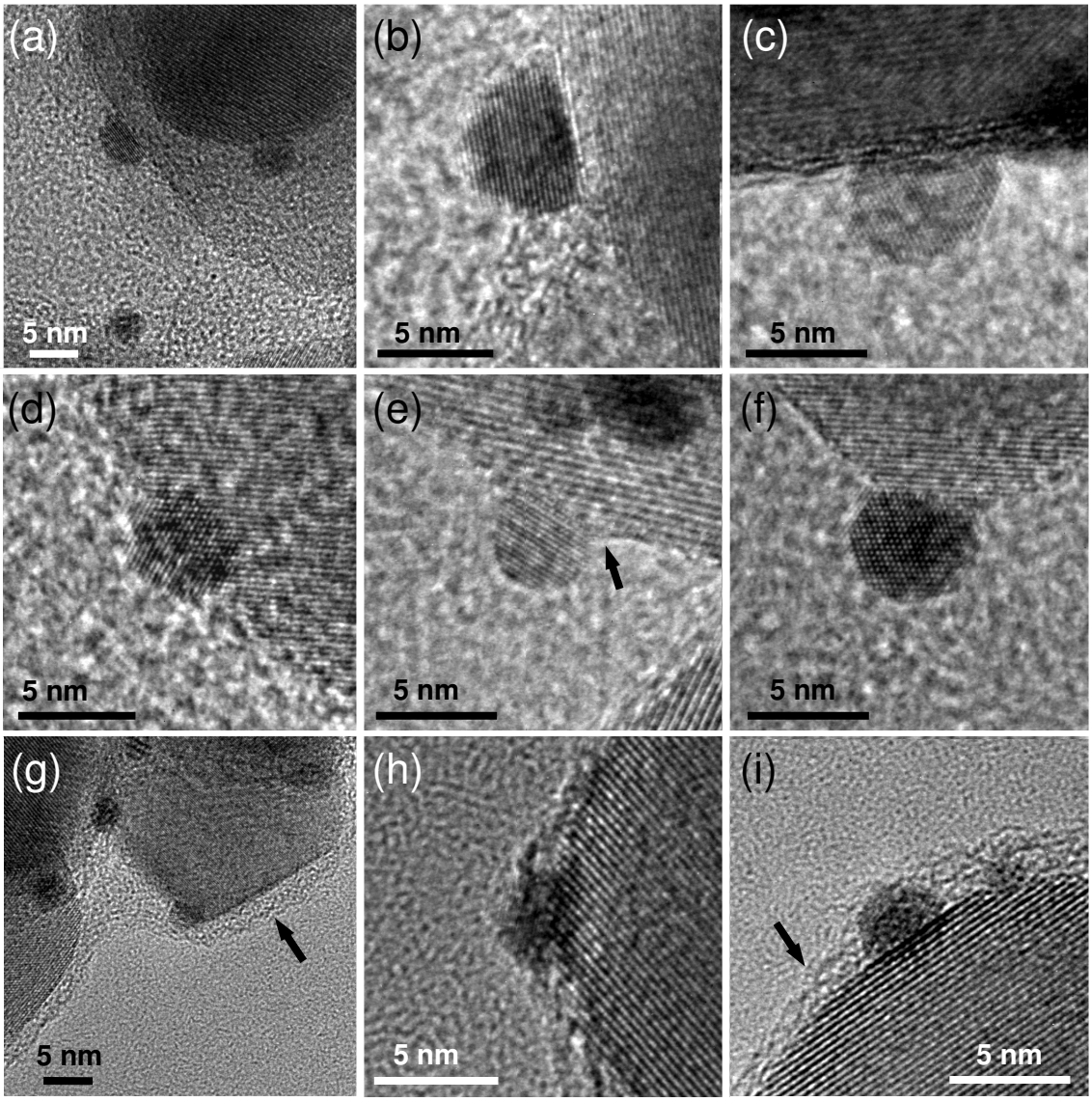

Croy et al. Fig. 2

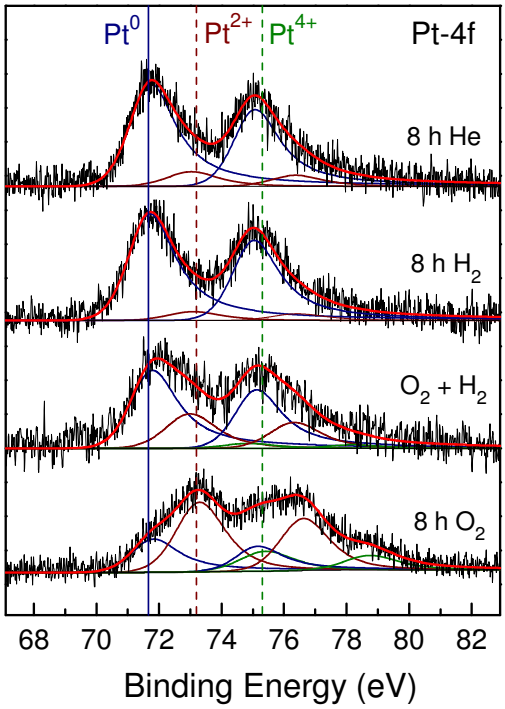

Croy et al., Fig. 3

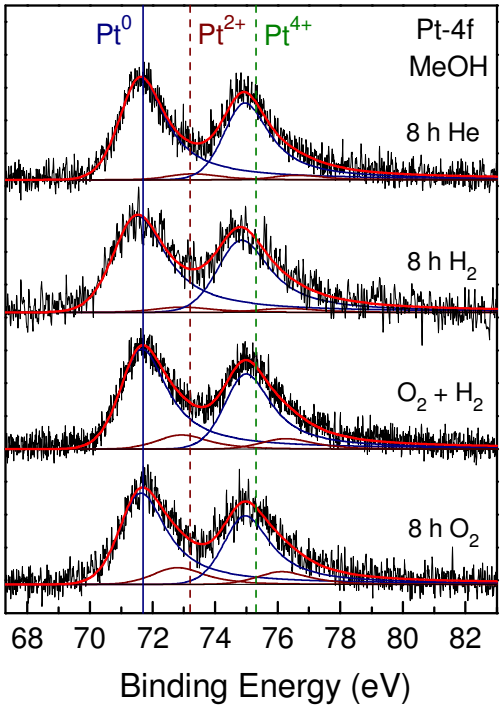

Croy et al., Fig. 4

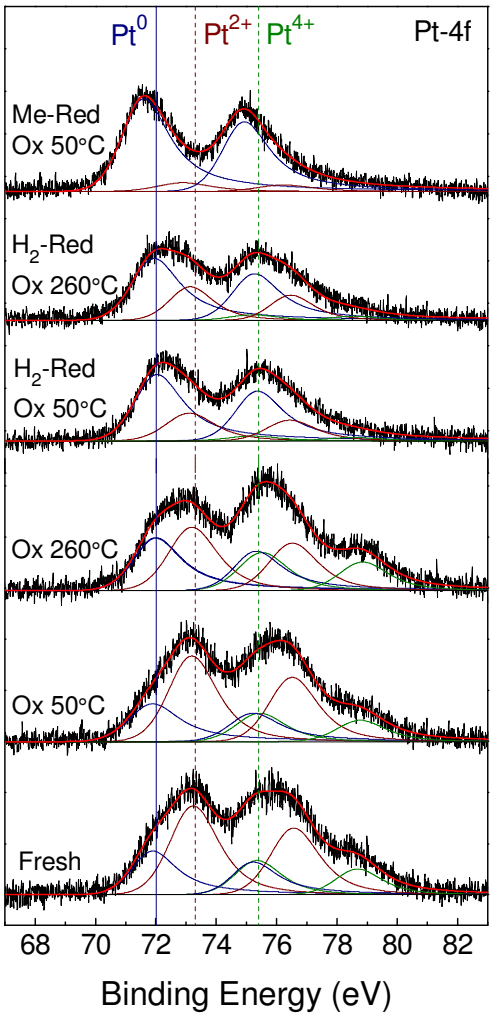

Croy et al., Fig. 5

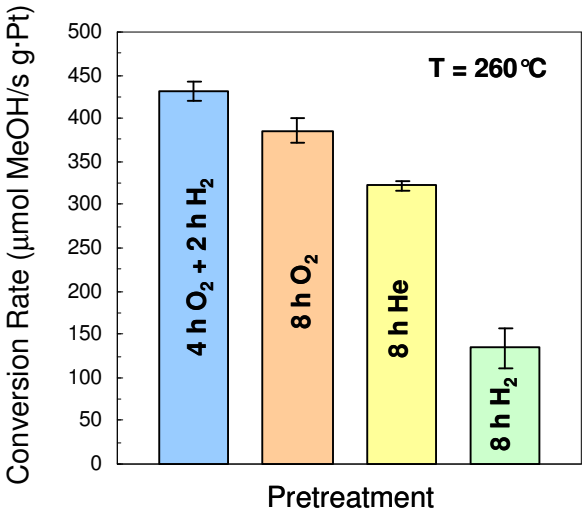

Croy et al., Fig. 6

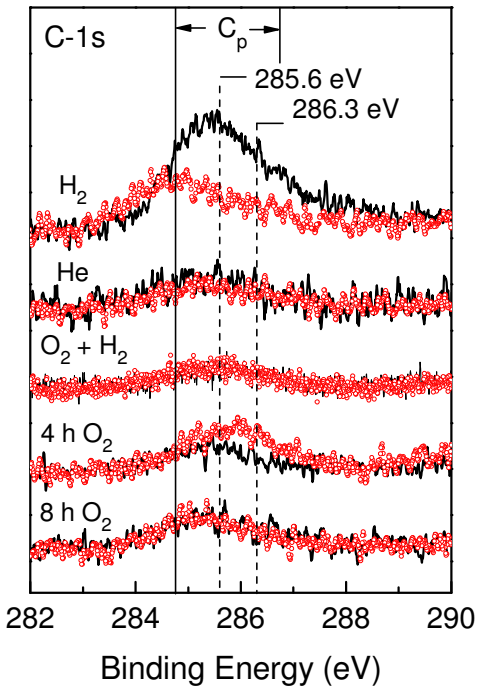

Croy et al., Fig. 7

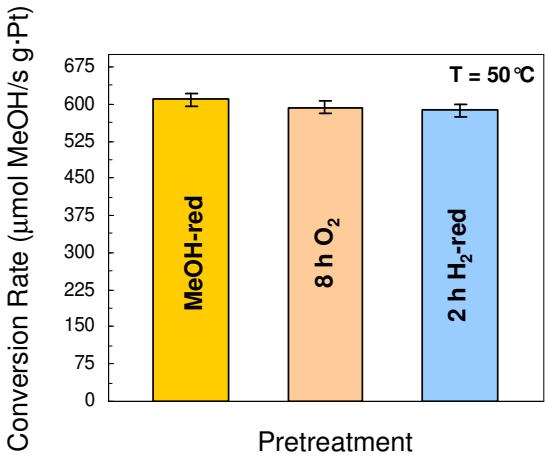

Croy et al., Fig. 8